# INCOMPRESSIBLE FLOW PAST A CIRCULAR CYLINDER: DEPENDENCE OF THE COMPUTED FLOW FIELD ON THE LOCATION OF THE LATERAL BOUNDARIES[†]

M. Behr, D. Hastreiter, S. Mittal and T.E. Tezduyar
AEM/AHPCRC
Supercomputer Institute
University of Minnesota
1200 Washington Avenue South
Minneapolis, MN 55415

July 26, 1994
Revised: September 27, 1994

## Abstract

The influence of the location of the lateral boundaries on 2D computation of unsteady incompressible flow past a circular cylinder is investigated. The case of Reynolds number 100 is used as a benchmark, and several quantities characterizing the unsteady flow are obtained for a range of lateral boundary locations. The computations are performed with two distinct finite element formulations – space-time velocity-pressure formulation and velocity-pressure-stress formulation. We conclude that the distance between the cylinder and the lateral boundaries can have a significant effect on the Strouhal number and other flow quantities. The minimum distance at which this influence vanishes has been found to be larger than what is commonly assumed.

## 1. Introduction

One of the standard aspects of numerical simulation is the selection of the computational domain, which is often only an approximation of the actual domain of the physical problem. Many of the types of boundary conditions used in practical applications are applicable only if they are sufficiently removed from the region where accuracy of the solution is important. The desire to limit computational cost, on the other hand, provides motivation to reduce the domain size. As usual, the best results can be expected when these contradictory tendencies are optimally balanced.

The issue of proper placement of the boundaries arose several times in our past computations, receiving the fullest attention in the benchmark 2D studies involving incompressible flow past a circular cylinder at Reynolds number 100. This transient problem is frequently

[†]This research was sponsored by NASA-JSC under grant NAG 9-449, by NSF under grants CTS-8796352 and ASC-9211083, by ARPA under NIST contract 60NANB2D1272, and by ARO under grant DAAH04-93-G-0514. Partial support for this work has also come from the ARO contract number DAAL03-89-C-0038 with the AHPCRC at the University of Minnesota.

used to assess the accuracy of finite element formulations, as it is characterized by a handful of well known quantities, such as the mean drag coefficient, or a nondimensional frequency of the vortex shedding known as the Strouhal number. At this low Reynolds number, such characteristic quantities obtained with the 2D numerical approach should approximate closely the values obtained experimentally, e.g., by Roshko [1].

It was one of our early observations regarding this problem that the shedding characteristics, and the Strouhal number in particular, is significantly affected by the dissipation introduced by the time-integration scheme. In reference [2], a dissipative T1 time-stepping scheme was compared against a T6 scheme, as well as a vorticity-stream function solution. The T6 scheme gains accuracy over the T1 scheme by a more selective application of the stabilization terms. Reasonably good values of the Strouhal number were obtained with the T6 scheme and the vorticity-stream function formulation. The T1 scheme however, produced noticeably low shedding frequency, and thus, a *low* Strouhal number. Also seen were lower than normal values of the average drag coefficient, as well as lower amplitude of the lift coefficient. These effects were observed for the Q1P0 (bilinear velocity, constant discontinuous pressure) element. Interestingly, the Q1Q1 (equal-order bilinear interpolation for both fields) element used in [3], again in the context of a T1 and a T6 scheme, did not exhibit such sensitivity. The conclusion that choice of the transient algorithm can significantly influence the quantities characterizing an unsteady flow field did not rule out the possibility that similar shifts in Strouhal number can be caused by other aspects of the numerical method, such as the aforementioned choice of the size of the computational domain.

In conjunction with the two international symposia devoted to this subject (University of Wales, Swansea, Wales, July 1989; Stanford University, Stanford, California, July 1991), we have examined the effect of the location and type of the outflow, or downstream, boundary. These studies were first performed with the velocity-pressure formulation [4], and then with the vorticity-stream function formulation [5]. It was found that with the commonly used traction-free boundary condition applied at the outflow boundary, the Strouhal number and other quantities are quite insensitive to the distance of that boundary from the cylinder. They were observed to deviate from the expected values only as the said distance is reduced below 6 cylinder diameters. Below that value, the change in the flow behavior is rather dramatic with the solution losing its periodicity and tending to a steady-state. Because of a need for accurate representation of a wake behind bluff bodies, in most computations reported in the literature, the downstream boundary is placed much farther downstream than the critical distance found in [4, 5]. The situation is not as clear regarding the positioning of the other boundaries of the computational domain.

A small set of experiments described in the present article shows that the shedding solution is far more sensitive to the location of the lateral boundaries. We obtain a series of flow fields around the cylinder, with two independent formulations of Navier-Stokes equations, and with a set of five domains, with varying distance separating the lateral boundaries from the cylinder. When constructing the meshes for the different domains, the same inner mesh is used, with an appropriate number of extension elements added at the lateral boundaries. This is the same approach as the one used in [4, 5]. The data presented here suggests that the lateral boundaries should be distanced from the cylinder by at least 8 cylinder diameters in order to remove the influence of those boundaries on the shedding phenomena. In particular, Strouhal number can become artificially *high* when the lateral boundaries are placed too

close to the cylinder. The difference in the boundary location may have caused the discrepancy between the Strouhal number obtained for the cylinder problem in [6] with a one-step time-integration, and the T1 result reported in [2]. In fact, it has not been unusual for the past computations of this benchmark problem, including a recent comparison of transient algorithms [7], to be performed with the lateral boundaries placed as close as 4.5 cylinder diameters away. Such low values might have influenced the measured Strouhal number and other flow quantities. It is our belief that lateral boundaries should be positioned farther apart, especially when the nature of a time-integration scheme is under investigation. In cases where the zone of influence of the lateral boundaries is difficult to predict, and when the shedding quantities are used as an accuracy indicator, a check on the influence of the boundary placement is as important as the traditional mesh refinement comparison. It is possible to envision situations where the dissipative effect of the transient algorithm (lowering the Strouhal number) combines with the constraining effect of the closely spaced lateral boundaries (increasing the Strouhal number), to produce shedding characteristics which are close to target experimental observations, yet are not indicative of overall accuracy of the solution method.

In Section 2 we state briefly the physical problem under consideration. In Section 3 we recall the velocity-pressure and velocity-pressure-stress formulations. We present the results of the numerical tests in Section 4, and reiterate main points of this study in Section 5.

## 2. Governing Equations

In this section, we state the problem in the form of Navier-Stokes equations of incompressible flows. In the following, $\Omega_t \subset R^{n_{\rm sd}}$ will denote a bounded region at time $t \in (0,T)$, with boundary $\Gamma_t$, where $n_{\rm sd}$ is the number of space dimensions. The time index indicates that the domain may be deforming. The symbols $\mathbf{u}(\mathbf{x},t)$ and $p(\mathbf{x},t)$ will represent the velocity and pressure fields, respectively. The external forces, such as the gravity, will be represented by $\mathbf{f}(\mathbf{x},t)$. The Navier-Stokes equations for incompressible flows are

$$\rho\left(\frac{\partial \mathbf{u}}{\partial t} + \mathbf{u}\cdot\boldsymbol{\nabla}\mathbf{u} - \mathbf{f}\right) - \boldsymbol{\nabla}\cdot\boldsymbol{\sigma} = \mathbf{0} \qquad \text{on } \Omega_t \quad \forall t \in (0,T), \tag{1}$$

$$\boldsymbol{\nabla}\cdot\mathbf{u} = 0 \qquad \text{on } \Omega_t \quad \forall t \in (0,T), \tag{2}$$

where $\rho$ is the density assumed to be constant. For the Newtonian flows under consideration here, the stress tensor for a fluid with dynamic viscosity $\mu$ is defined as follows:

$$\boldsymbol{\sigma} = -p\mathbf{I} + \mathbf{T}, \quad \mathbf{T} = 2\mu\boldsymbol{\varepsilon}(\mathbf{u}). \tag{3}$$

This equation set is completed by suitable boundary conditions and an initial condition consisting of a divergence-free velocity field specified over the entire domain:

$$\mathbf{u}(\mathbf{x},0) = \mathbf{u}_0, \quad \boldsymbol{\nabla}\cdot\mathbf{u}_0 = 0 \quad \text{on } \Omega_0. \tag{4}$$

The boundary conditions consist of a uniform velocity profile specified at the inflow boundary, no-slip condition at the cylinder surface, flow symmetry conditions at the lateral boundaries, and traction-free condition at the outflow boundary.

## 3. Finite Element Formulations

In this section we outline the two finite element formulations used to conduct the numerical tests described in Section 4. It should be noted that both formulations were designed to deal with problems more complex than the one under consideration in this paper. The space-time formulation is suitable for problems involving moving boundaries and interfaces, while the velocity-pressure-stress formulation is typically used to solve flow problems which involve non-Newtonian constitutive relations.

### 3.1. Space-Time Velocity-Pressure Formulation

In a space-time formulation, the space-time domain is first divided into a sequence of space-time slabs $Q_n$, and each slab is decomposed into space-time elements $Q_n^e$. A slab $Q_n$ is located between the time levels $t_n$ and $t_{n+1}$. The integration of a functional over a slab will include integration over both the spatial domain $\Omega_t$ and the temporal one $[t_n, t_{n+1}]$. Since many of the functions to be introduced here will be discontinuous across slab interfaces, we will employ the notation $(\cdot)_n^-$ and $(\cdot)_n^+$ to indicate the values at $t_n$ as it is approached from below and above, respectively. The number of elements in slab $n$ is written as $(n_{\rm el})_n$. The finite element formulation begins with choosing appropriate trial solution ($(\mathcal{S}_{\mathbf{u}}^h)_n$ and $(\mathcal{S}_p^h)_n$) and weighting function ($(\mathcal{V}_{\mathbf{u}}^h)_n$ and $(\mathcal{V}_p^h)_n = (\mathcal{S}_p^h)_n$) spaces for the velocity and pressure. In our computations we employ piecewise linear functions for all fields.

The stabilized space-time formulation for deforming domains can be written as follows: given $(\mathbf{u}^h)_n^-$, find $\mathbf{u}^h \in (\mathcal{S}_{\mathbf{u}}^h)_n$ and $p^h \in (\mathcal{S}_p^h)_n$ such that $\forall \mathbf{w}^h \in (\mathcal{V}_{\mathbf{u}}^h)_n$ and $\forall q^h \in (\mathcal{V}_p^h)_n$

$$
\begin{aligned}
&\int_{Q_n} \mathbf{w}^h \cdot \rho \left( \frac{\partial \mathbf{u}^h}{\partial t} + \mathbf{u}^h \cdot \boldsymbol{\nabla} \mathbf{u}^h - \mathbf{f} \right) dQ + \int_{Q_n} \boldsymbol{\varepsilon}(\mathbf{w}^h) : \boldsymbol{\sigma}(p^h, \mathbf{u}^h) dQ \\
&+ \int_{Q_n} q^h \boldsymbol{\nabla} \cdot \mathbf{u}^h dQ + \int_{\Omega_n} (\mathbf{w}^h)_n^+ \cdot \rho \left( (\mathbf{u}^h)_n^+ - (\mathbf{u}^h)_n^- \right) d\Omega \\
&+ \sum_{e=1}^{(n_{\rm el})_n} \int_{Q_n^e} \tau_{\rm MOM} \frac{1}{\rho} \left[ \rho \left( \frac{\partial \mathbf{w}^h}{\partial t} + \mathbf{u}^h \cdot \boldsymbol{\nabla} \mathbf{w}^h \right) - \boldsymbol{\nabla} \cdot \boldsymbol{\sigma}(q^h, \mathbf{w}^h) \right] \\
&\quad \cdot \left[ \rho \left( \frac{\partial \mathbf{u}^h}{\partial t} + \mathbf{u}^h \cdot \boldsymbol{\nabla} \mathbf{u}^h - \mathbf{f} \right) - \boldsymbol{\nabla} \cdot \boldsymbol{\sigma}(p^h, \mathbf{u}^h) \right] dQ \\
&+ \sum_{e=1}^{(n_{\rm el})_n} \int_{Q_n^e} \tau_{\rm CONT} \boldsymbol{\nabla} \cdot \mathbf{w}^h \, \rho \boldsymbol{\nabla} \cdot \mathbf{u}^h dQ = \int_{(P_n)_{\boldsymbol{h}}} \mathbf{w}^h \cdot \boldsymbol{h}^h dP. \qquad (5)
\end{aligned}
$$

Here $\boldsymbol{h}^h$ represents the Neumann boundary condition imposed, $(P_n)_{\boldsymbol{h}}$ is the part of the slab boundary with such conditions, and $\tau_{\rm MOM}$ and $\tau_{\rm CONT}$ are the stabilization parameters. The solution to (5) is obtained sequentially for all space-time slabs $Q_1, Q_2, \ldots, Q_{N-1}$, and the computations start with

$$
(\mathbf{u}^h)_0^- = \mathbf{u}_0^h. \qquad (6)
$$

In the formulation given by equation (5), the first four integrals, together with the right-hand-side, represent the time-discontinuous Galerkin formulation of (1)-(2). The fourth integral

enforces, weakly, the continuity of the velocity field in time. The two series of element-level integrals in the formulation are the least-squares stabilization terms. The reader can refer to [8–10] for further details regarding the space-time formulation for incompressible flows, including definitions of the stabilization parameters.

### 3.2. Velocity-Pressure-Stress Formulation

The velocity-pressure-stress formulation presented here is a restriction of the general formulation presented in [11], which was applicable to Oldroyd-B and Maxwell-B fluids, to the case of Newtonian fluids. In contrast to the space-time formulation presented in the preceding subsection, the 3 (or 6 in three dimensions) independent components of the extra stress tensor $\mathbf{T}$ are treated as additional unknowns, and the constitutive equation enters the variational formulation directly. The case of deforming domains is not covered here, so the subscripts denoting domain time level are dropped. Following the selection of suitable trial solution ($\mathcal{S}^h_{\mathbf{u}}$, $\mathcal{S}^h_p$ and $\mathcal{S}^h_{\mathbf{T}}$) and weighting function ($\mathcal{V}^h_{\mathbf{u}}$, $\mathcal{V}^h_p = \mathcal{S}^h_p$ and $\mathcal{V}^h_{\mathbf{T}} = \mathcal{S}^h_{\mathbf{T}}$) spaces for the velocity, pressure and the extra stress, the formulation can be written as follows: find $\mathbf{u}^h \in \mathcal{S}^h_{\mathbf{u}}$, $p^h \in \mathcal{S}^h_p$ and $\mathbf{T}^h \in \mathcal{S}^h_{\mathbf{T}}$ such that:

$$
\begin{aligned}
&\int_\Omega \mathbf{w}^h \cdot \rho \left( \frac{\partial \mathbf{u}^h}{\partial t} + \mathbf{u}^h \cdot \boldsymbol{\nabla} \mathbf{u}^h - \mathbf{f} \right) d\Omega - \int_\Omega \boldsymbol{\nabla} \cdot \mathbf{w}^h p^h d\Omega + \int_\Omega \boldsymbol{\varepsilon}(\mathbf{w}^h) : \mathbf{T}^h d\Omega \\
&- \int_{\Gamma_{\boldsymbol{h}}} \mathbf{w}^h \cdot \boldsymbol{h}^h d\Gamma d\Omega + \int_\Omega q^h \boldsymbol{\nabla} \cdot \mathbf{u}^h d\Omega \\
&+ \frac{1}{2\mu} \int_\Omega \mathbf{S}^h : \mathbf{T}^h d\Omega - \int_\Omega \mathbf{S}^h : \boldsymbol{\varepsilon}(\mathbf{u}^h) d\Omega \\
&+ \sum_{e=1}^{n_{\mathrm{el}}} \int_{\Omega^e} \tau_{\mathrm{MOM}} \frac{1}{\rho} \left[ \rho \left( \frac{\partial \mathbf{w}^h}{\partial t} + \mathbf{u}^h \cdot \boldsymbol{\nabla} \mathbf{w}^h \right) + \boldsymbol{\nabla} q^h - \boldsymbol{\nabla} \cdot \mathbf{S}^h \right] \\
&\qquad \cdot \left[ \rho \left( \frac{\partial \mathbf{u}^h}{\partial t} + \mathbf{u}^h \cdot \boldsymbol{\nabla} \mathbf{u}^h - \mathbf{f} \right) + \boldsymbol{\nabla} p^h - \boldsymbol{\nabla} \cdot \mathbf{T}^h \right] d\Omega \\
&+ \sum_{e=1}^{n_{\mathrm{el}}} \int_{\Omega^e} \tau_{\mathrm{CONS}} 2\mu \left[ \frac{1}{2\mu} \mathbf{S}^h - \boldsymbol{\varepsilon}(\mathbf{w}^h) \right] : \left[ \frac{1}{2\mu} \mathbf{T}^h \boldsymbol{\varepsilon}(\mathbf{u}^h) \right] d\Omega \\
&+ \sum_{e=1}^{n_{\mathrm{el}}} \int_{\Omega^e} \tau_{\mathrm{CONT}} \, \boldsymbol{\nabla} \cdot \mathbf{w}^h \rho \, \boldsymbol{\nabla} \cdot \mathbf{u}^h d\Omega = 0, \quad \forall \mathbf{w}^h \in \mathcal{V}^h_{\mathbf{u}}, \quad \forall q^h \in \mathcal{V}^h_p, \quad \forall \mathbf{S}^h \in \mathcal{V}^h_{\mathbf{T}}. \qquad (7)
\end{aligned}
$$

In the computations that follow, formulation (7) has been time-discretized with the Crank-Nicholson scheme. Piecewise bilinear interpolations are used for all fields in the computations reported here. Further details of this formulation, including the design of the parameters $\tau_{\mathrm{CONS}}, \tau_{\mathrm{MOM}}$ and $\tau_{\mathrm{CONT}}$ can be found in [11, 12].

## 4. Tests

In this section, we describe our numerical tests which involve the standard benchmark problem of unsteady 2D flow past a cylinder at Reynolds number 100. The problem domain is

| Mesh | Distance A (see Figure 1) | Number of nodes | Number of elements |
|---|---|---|---|
| M090 | 9.0 | 3681 | 3540 |
| M125 | 12.5 | 4605 | 4450 |
| M160 | 16.0 | 5529 | 5360 |
| M240 | 24.0 | 7641 | 7440 |
| M320 | 32.0 | 9753 | 9520 |

Table 1. The mesh parameters.

shown in Figure 1.

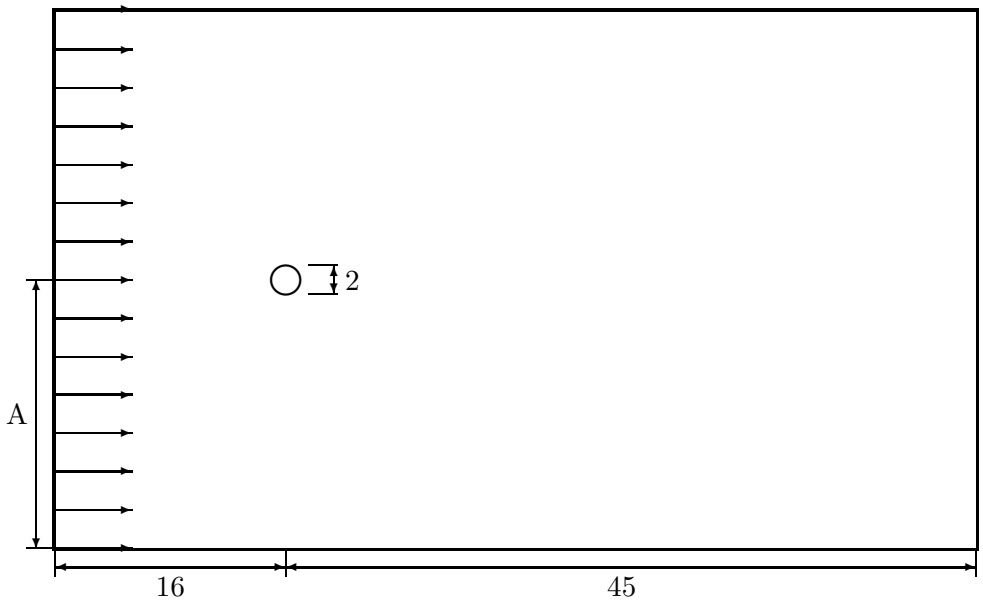


Figure 1. The computational domain.

The inflow velocity is specified as 1.0 at the inflow (leftmost) boundary. A no-slip condition is specified at the cylinder surface, zero normal velocity and zero tangential stress is assumed at the lateral boundaries, and a traction-free condition is prescribed at the outflow boundary. The distance of the upstream and downstream boundaries from the cylinder is fixed at the values shown in Figure 1 and deemed sufficient on the basis of the results presented in [4, 5]. The distance A is the subject of the current investigation. For this purpose, we employ a series of 5 meshes with A ranging from 9 to 32. These meshes will be referred to by symbols given in Table 1. To remove any dependence on near-field refinement, the meshes are nested, i.e., each smaller mesh can be viewed as a truncation of the next larger mesh.

Both formulations given in Section 3 are used to obtain periodic solutions on these five different meshes. A time step of 0.125, providing a resolution of approximately 100 time steps per vortex shedding period, is selected. Our previous experience [2] indicates that the refinement of the mesh is sufficient to obtain reliable measurements of the flow quantities. In all five cases, in order to shorten the computation time, a closest available periodic solution is either adapted or interpolated, and used as an initial condition. After the fully periodic

solution is reached, we measure and report the amplitude of the lift coefficient, average value of the drag coefficient and the Strouhal number. The amplitude of the lift coefficient is given in Table 2 and plotted in Figure 2. The mean drag coefficient is given in Table 3 and plotted in Figure 3. Finally, the Strouhal number is reported in Table 4 and plotted in Figure 4.

It can be clearly observed that both formulations, which are very different, show the same kind of dependence of the reported flow quantities on the position of the lateral boundaries. When the distance A is as small as 9.0, we see a 6% increase in the amplitude of the lift coefficient and the mean drag coefficient. The increase in the Strouhal number reaches 5%. It is apparent from the plots in Figures 2, 3 and 4, that these quantities stabilize within 1% of the final values only as the distance A exceeds 16.0. While there is a visible difference between the results from the two different formulations, both of them exhibit the same trend as the distance of the lateral boundary is varied. In particular, the variation in the Strouhal number due to the distance A being changed from 9.0 to 32.0, is at least twice of the difference in Strouhal number for the two formulations obtained at a fixed value of A.

## 5. Concluding Remarks

We have recalled the role of vortex shedding from a cylinder as a benchmark frequently employed to study the accuracy of a numerical scheme. The most notable quantities which characterize the vortex shedding are the amplitude of the lift coefficient, mean drag coefficient and the Strouhal number. These quantities played important role in our past computations which sought to determine the correct placement of the downstream boundary. They are also frequently employed to assess the accuracy of time-integration algorithms. In this study, we concentrated on the dependence of the vortex shedding phenomena on the placement of the lateral boundaries. The results we obtained indicate that the distance between the lateral boundaries and the cylinder beyond which the presence of these artificial boundaries ceases to influence the Strouhal number and other quantities, is greater than what is commonly assumed. Cautious placement of the lateral boundaries is advocated, especially when the Strouhal number and its deviation from experimentally obtained value is used to draw conclusions about other aspects of the numerical algorithm. In particular, we find that the lateral boundaries should be removed from the cylinder by a distance of 8 cylinder diameters. If this is not the case, the computed Strouhal number will have an artificially high value.

| Mesh | Amplitude of the Lift Coefficient | |
|---|---|---|
| | Space-Time Velocity-Pressure | Velocity-Pressure-Stress |
| M090 | 0.3946 | 0.3880 |
| M125 | 0.3794 | 0.3739 |
| M160 | 0.3743 | 0.3692 |
| M240 | 0.3709 | 0.3666 |
| M320 | 0.3706 | 0.3659 |

Table 2. Variation of the amplitude of the lift coefficient.

| Mesh | Mean Drag Coefficient | |
|---|---|---|
| | Space-Time Velocity-Pressure | Velocity-Pressure-Stress |
| M090 | 1.4552 | 1.4732 |
| M125 | 1.4023 | 1.4214 |
| M160 | 1.3836 | 1.4030 |
| M240 | 1.3721 | 1.3917 |
| M320 | 1.3698 | 1.3894 |

Table 3. Variation of the mean drag coefficient.

| Mesh | Strouhal Number | |
|---|---|---|
| | Space-Time Velocity-Pressure | Velocity-Pressure-Stress |
| M090 | 0.1711 | 0.1739 |
| M125 | 0.1658 | 0.1690 |
| M160 | 0.1641 | 0.1672 |
| M240 | 0.1624 | 0.1661 |
| M320 | 0.1624 | 0.1661 |

Table 4. Variation of the Strouhal number.

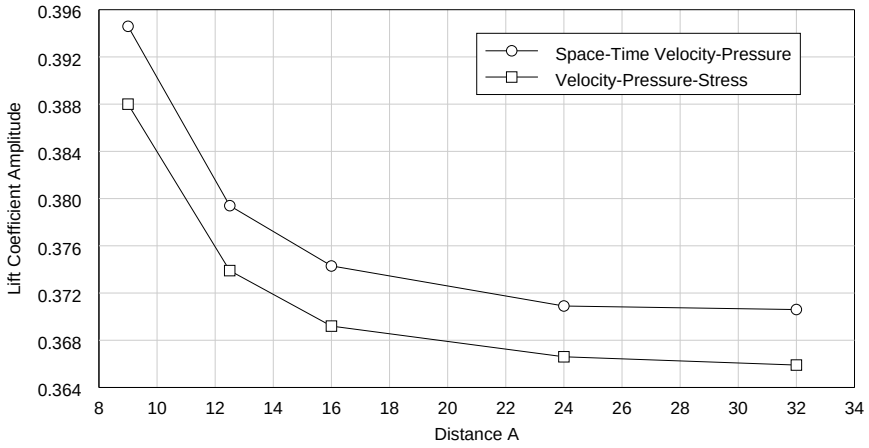


Figure 2. Variation of the amplitude of the lift coefficient with distance A.

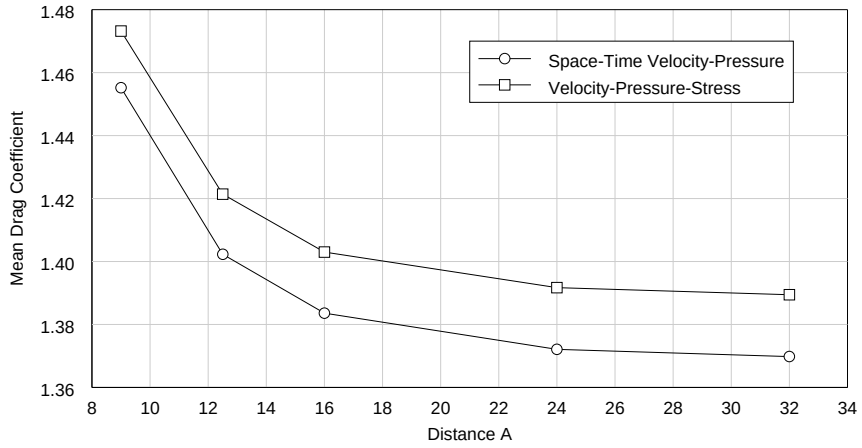


Figure 3. Variation of the mean drag coefficient with distance A.

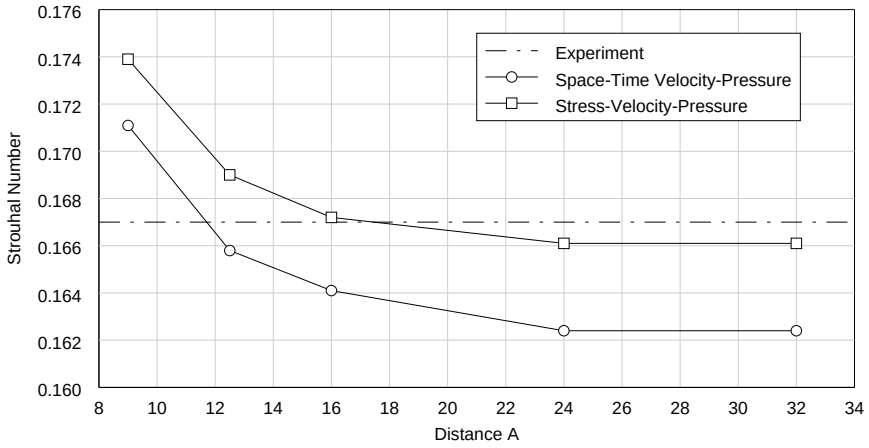


Figure 4. Variation of the Strouhal number with distance A.

## References

[1] A. Roshko, "On the development of turbulent wakes from vortex streets", NACA Report 1191, NACA, 1954.

[2] T.E. Tezduyar, J. Liou, and D.K. Ganjoo, "Incompressible flow computations based on the vorticity-stream function and velocity-pressure formulations", *Computers & Structures*, **35** (1990) 445–472.

[3] T.E. Tezduyar, "Stabilized finite element formulations for incompressible flow computations", *Advances in Applied Mechanics*, **28** (1991) 1–44.

[4] T.E. Tezduyar and R. Shih, "Numerical experiments on downstream boundary of flow past cylinder", *Journal of Engineering Mechanics*, **117** (1991) 854–871.

[5] M. Behr, J. Liou, R. Shih, and T.E. Tezduyar, "Vorticity-stream function formulation of unsteady incompressible flow past a cylinder: Sensitivity of the computed flow field to the location of the outflow boundary", *International Journal for Numerical Methods in Fluids*, **12** (1991) 323–342.

[6] A.N. Brooks and T.J.R. Hughes, "Streamline upwind/Petrov-Galerkin formulations for convection dominated flows with particular emphasis on the incompressible Navier-Stokes equations", *Computer Methods in Applied Mechanics and Engineering*, **32** (1982) 199–259.

[7] J. Simo and F. Armero, "Unconditional stability and long-term behavior of transient algorithms for the incompressible Navier-Stokes and Euler equations", to appear in *Computer Methods in Applied Mechanics and Engineering*, 1994.

[8] T.E. Tezduyar, M. Behr, and J. Liou, "A new strategy for finite element computations involving moving boundaries and interfaces – the deforming-spatial-domain/space-time procedure: I. The concept and the preliminary tests", *Computer Methods in Applied Mechanics and Engineering*, **94** (1992) 339–351.

[9] T.E. Tezduyar, M. Behr, S. Mittal, and J. Liou, "A new strategy for finite element computations involving moving boundaries and interfaces – the deforming-spatial-domain/space-time procedure: II. Computation of free-surface flows, two-liquid flows, and flows with drifting cylinders", *Computer Methods in Applied Mechanics and Engineering*, **94** (1992) 353–371.

[10] M. Behr and T.E. Tezduyar, "Finite element solution strategies for large-scale flow simulations", *Computer Methods in Applied Mechanics and Engineering*, **112** (1994) 3–24.

[11] M. Behr, *Stabilized Finite Element Methods for Incompressible Flows with Emphasis on Moving Boundaries and Interfaces*, Ph.D. thesis, Department of Aerospace Engineering and Mechanics, University of Minnesota, 1992.

[12] M. Behr, L.P. Franca, and T.E. Tezduyar, "Stabilized finite element methods for the velocity-pressure-stress formulation of incompressible flows", *Computer Methods in Applied Mechanics and Engineering*, **104** (1993) 31–48.